Published in final edited form as:

Bioorg Med Chem Lett. 2020 February 15; 30(4): 126899. doi:10.1016/j.bmcl.2019.126899.

Discovery of small molecule antagonists of chemokine receptor CXCR6 that arrest tumor growth in SK-HEP-1 mouse xenografts as a model of hepatocellular carcinoma

Satyamaheshwar Peddibhotla[a,*], **Paul M. Hershberger**[a], **R. Jason Kirby**[a], **Eliot Sugarman**[a], **Patrick R. Maloney**[a], **E. Hampton Sessions**[a], **Daniela Divlianska**[a], **Camilo J. Morfa**[a], **David Terry**[a], **Anthony B. Pinkerton**[a], **Layton H. Smith**[a], **Siobhan Malany**[a,b,*]

[a]Conrad Prebys Center for Chemical Genomics, Sanford Burnham Prebys Medical Discovery Institute, La Jolla, CA 92037, USA

[b]College of Pharmacy, University of Florida, 1345 Center Drive, Gainesville, FL 32610, USA

Abstract

The chemokine system plays an important role in mediating a proinflammatory microenvironment for tumor growth in hepatocellular carcinoma (HCC). The CXCR6 receptor and its natural ligand CXCL16 are expressed at high levels in HCC cell lines and tumor tissues and receptor expression correlates with increased neutrophils in these tissues contributing to poor prognosis in patients. Availability of pharmacologcal tools targeting the CXCR6/CXCL16 axis are needed to elucidate the mechanism whereby neutrophils are affected in the tumor environment. We report the discovery of a series of small molecules with an *exo*-[3.3.1]azabicyclononane core. Our lead compound **81** is a potent (EC_{50} = 40 nM) and selective orally bioavailable small molecule antagonist of human CXCR6 receptor signaling that significantly decreases tumor growth in a 30-day mouse xenograft model of HCC.

Keywords

CXCR6 receptor antagonist; Hepatocellular carcinoma; SK-HEP xenograft model; B-arrestin signaling; Azabicyclononane scaffold

CXCR6 is a seven transmembrane domain G protein–coupled receptor (GPCR) target for the natural ligand, CXCL16, a chemokine that exists in both membrane-anchored and soluble variant forms to regulate leukocyte trafficking during cellular stress. CXCR6 receptor is expressed on many cell types in the immune system including dendritic cells, CD4+ cells, CD8+ cells, natural killer cells and natural killer T cells.[1–3] The CXCR6/CXCL16 axis plays

*Corresponding authors at: Conrad Prebys Center for Chemical Genomics, Sanford Burnham Prebys Medical Discovery Institute, La Jolla, CA 92037, USA (S. Malany). peddibhotlas@seminolestate.edu (S. Peddibhotla), smalany@cop.ufl.edu (S. Malany).

Declaration of Competing Interest

The authors declare that they have no known competing financial interests or personal relationships that could have appeared to influence the work reported in this paper.

Appendix A.: Supplementary data

Supplementary data to this article can be found online at http://doi.org/10.1016/j.bmcl.2019.126899.

a critical role in proinflammatory cytokine expression in liver that may induce CXCR6 immune-dependent mechanism in hepatocarcinogenesis. CXCR6 and CXCL16 are highly expressed in many types of human cancers including hepatocellular carcinoma (HCC),[4] a cancer that ranks fifth in frequency worldwide among all malignancies and is the third leading cause of cancer mortality.[5] CXCR6 is consistently expressed in all eight hepatoma cell lines reported.[6] The expression profile is low in normal hepatocytes, increases in noninvasive HCC cells, and reaches highest levels in invasive HCCs. Upregulation of CXCR6 receptor contributes to a proinflammatory tumor microenvironment that promotes metastasis and has been identified as an independent predictor for increased recurrence and poor survival in patients with HCCs.[6,7] In agreement, genetic downregulation of CXCR6 receptor inhibited HCC cell invasion *in vitro* and in mice subcutaneous xenografts, inhibited tumorigenicity, neutrophil recruitment, angiogenesis, and metastasis of hepatoma cells.[6] Verifying the therapeutic impact of CXCR6 in HCC has been hampered by lack of available small molecule probes. Thus, the development of pharmacologically available small molecule antagonists to CXCR6/CXCL16 signaling that reduce inflammation in the liver or modulate the immune response may provide an avenue to ameliorate hepatic tumor progression and metastasis and represent promising therapeutics for HCC and related cancers. We report the discovery of the first potent, selective orally bioavailable small molecule antagonist of the CXCR6 receptor signaling that decreases tumor growth in a mouse xenograft model of HCC.

We previously reported the discovery of an initial series of CXCR6 receptor antagonists represented by probe compound **17** (**ML339**, Table 1)[8] through high throughput screening (HTS) of the NIH Molecular Library Small Molecular Repository (MLSMR), medicinal chemistry and structure-activity relationship (SAR) studies as a first in class small molecule probe. Compound **17** is potent in antagonizing (β-arrestin recruitment and cAMP signaling of the human CXCR6 receptor induced by CXCL16 (IC_{50} = 0.3 and 1.4 μM, respectively) and is devoid of activity against the CCR6, CXCR5, and CXCR4 human receptors (IC_{50} > 80 μM).

From our probe discovery of compound **17**, we pursued a hit to lead program under the Florida Translational Research Program (FTRP) and report here an additional lead series distinct from compound **17** with improved potency in cell-based signaling as exemplified by compound **81** (Fig. 1, Table 3). Compound **81** has improved plasma stability and exhibited *in vivo* activity in a mouse xenograft model of HCC. The synthetic scheme for compound **81** is shown in the supplemental information.

Unless otherwise noted, compounds referred to in the text are listed in Table 1. The screening hit from the MLSMR library, compound **1**, had unassigned stereochemistry for the 3-amino group and was not defined as the *endo* or *exo* isomer. Hence synthesis of analogs (Scheme S1) and intial SAR study was designed to address the following key questions; a) is the [3.3.1]azabicyclononane core required for activity, b) is the reverse amide substituent in the *exo* or *endo* position in the primary hit compound **1**, c) is the *exo* or *endo* position essential or preferred, d) is the 3,4,5-trimethoxybenzoyl motif required and e) does substitution of the anilide group appended to the bridgehead nitrogen influence activity? Compound **1** was synthesized from the *exo-tert*-butyl-3-amino-9-azabicyclo[3.3.1]nonane-9-

carboxylate (CAS 1363380-67-9). The resynthesized batch recapitulated the activity of the screening hit and was identical by NMR to the commercial sample of the parent singleton hit and was further characterized by x-ray crystallography (Cambridge Structural Database CCDC 1969634) to unambiguously establish the *exo* stereochemistry at the 3,4,5-trimethoxybenzamide region of the molecule[8] (see Supporting Information).

Compound **2**, the 3-*endo* isomer was obtained from a building block which was a 1:1 mixture of *exo/endo* isomers, after separation by flash chromatography. Comparison of compounds **1** and **2** showed that for compounds with the [3.3.1] scaffold, the 3-*exo* stereochemistry was required for activity (compounds **1** and **2**). The same trend was noted for the less active [3.2.1] scaffold (compound **3** and **4**). The monocyclic 4-aminopiperidine analog (compound **5**) was inactive. These data prompted us to next explore aryl substitution at positions R^1 and R^2 in the anilide and benzamide moieties respectively in the scaffold. The completely unsubstituted analog (Entry **6**, $R^1 = R^2 = H$) was inactive. Electron withdrawing groups were preferred at the R^1 position. The 4-Cl analog was the most active and approximately four-fold better than the 4-H (compounds **1** and **8**). The SAR at the benzamide R^2 position was explored by varying R^2 to 3,4-dimethoxy, 3,5-dimethoxy, 3-methoxy, 4-methoxy, or 3,4-methyleneoxy and keeping R^1 = Cl. For these analogous sets, activity was only observed when R^2 was 3,4,5-trimethoxy (compounds **8** and **11**–**15**). Substitution at the 2-position was markedly better than at the 4-position, with the 2-OMe and 2-Cl analogs both being 10-fold better than the corresponding 4-OMe and 4-Cl analogs (compounds **7**–**10** vs **16**–**19**). The 2-Cl was the most potent closely followed by the 2-CN among the electron withdrawing groups at the 2-position (compounds **16**–**23**). At the 3-position the preference for an electron withdrawing group continued but with 2–3 fold lower potency (compounds **24**–**28**). Among the disubstituted analogs at R_1 position, analogs with a 2-Cl group were the most potent (compounds **29**–**34**). In contrast 2,6-disubstitution abolished activity possibly by moving the aromatic ring out of plane with respect to the amide group (compounds **32** and **36**). The 2-Cl analog (compound **17**) met the probe criteria and was scaled-up to be nominated as the probe **ML339** under the molecular libraries program.[8]

Our SAR strategy for further optimization of **ML339** to an *in vivo* active lead for proof of concept studies focused on keeping the *exo*-[3.3.1] bicycle intact and making broad changes in the anilide group, glycine (acetate) linker and the 3,4,5-trimethoxybenzamide portion of the molecule and then focused SAR follow up around the most potent leads obtained. Demethylation of 3,4,5-trimethoxyphenyl has been linked to poor metabolic stability and pharmacokinetic (PK) properties. Earlier attempts to address this potential liability by removing any of these OMe groups were not productive (compounds **8** and **11**–**15**). Keeping the more potent 2-Cl, R^1 substituent in ML339 constant, we systematically screened monomethoxy substituents at the R^2 position (compounds **37**–**39**, Supplementry Table 1) and found complete erosion of activity in the β-arrestin assay and only found borderline (EC_{50} = 15.1 μM) cAMP activity (compound **37**, R^2 = 2-OMe). Keeping 2-OMe constant at the R^2 position, we screened other electron withdrawing groups at the 2-position (R^1) and walked the Cl substituent to 3- and 4- position on the anilide group (compound **40**–**49**, Supplementry Table 1). There was no improvement in the cAMP activity except for the 4-Cl

(R^1) derivative as previously seen (compound **45** vs compounds **11**–**15**). Screening substituents other than methoxy at the R^2 position resulted in only a marginal increase in cAMP activity and continued loss of activity in the β-arrestin assay (compound **49**). This series of compounds was deprioritized based on its weak activity in the signaling assays.

We next looked at the glycine linker and found that replacement of the amide carbonyl with a flexible methylene group resulted in complete loss of activity in **ML339** (compound **50**, Supplementry Table 2). A conformationally more rigid linker with *gem*-dimethyl substitution led to significant or complete loss of activity in cAMP and β-arrestin assay respectively (compound **51**, Supplementry Table 2 vs compound **17**). Activity in cAMP assay improved 2-fold in 2-methoxybenzamide (R^2) vs the 3,4,5-trimethoxybenzamide (compound **51** and **52**, Supplementry Table 2). Walking the Cl (R^1) substituent or the OMe (R^2) around the aryl ring led to completely inactive analogs. This series of compounds was also deprioritized based on its weak activity observed in the cAMP assay.

The potential of toxicity resulting from hydrolysis of the aniline amide in compound **17** under physiological conditions prompted us to explore a series of analogs that replaced the anilide moiety with aryl methylene or heteroaryl methylene groups. Methoxyphenyl at the R position abolished activity (compounds **56**–**58**, Table 2). As before, electron withdrawing substituents seem to retain activity with the 2-chlorobenzyl derivative having the best activity (compound **59**, Table 2) albeit at 48-fold lower activity than compound **17**. Further exploration of bicyclic aryl and heteroaryl groups led to the 2-benzothiophenyl and 2-benzothiazolyl analogs with significant retention of activity in both β-arrestin and cAMP assays (compound **67**–**68**, Table 2). We recognized that the 2-benzothiazole analog compound 68 was a significant find, as it is a bio-isostere of the anilide group in compound **17**. The closely related bio-isosteric benzoxazole and benzimidazole analogs are also active however significantly less potent (compounds **69** and **70**, Table 2). Extending the methylene linker by one carbon in compound **71** or a carbonyl linkage in compound **72** led to a complete or 100-fold loss in activity, respectively (Table 2). These results point to specificity of interaction of the target with the 2-benzothiazole moiety.

In order to further improve the potency of compound **68**, we screened a limited set of substituents on the 2-benzothiazole moiety derived from commercially available substituted 2-chloromethylbenzothiazoles (compounds **73**–**76**, Table 3). All chlorobenzothiazole analogs had equipotent or improved activity over compound **68** (Table 2) and the 4-Cl derivative was the most potent in both β-arrestin and cAMP assays (compound **73**). Electron withdrawing groups were clearly preferred at the 4-position of the benzothiazole analogs in keeping with the observation for previous anilide series (compounds **73**, **77**–**79**, Table 3). Finally, 4-Br and 4-CF_3 groups offered significant further improvements in potency especially in the cAMP assay for the 4-CF_3 analog (compounds **80** and **81**, Table 3). Compound **81** became our lead compound with pIC_{50} = 7.4 ± 0.1 (IC_{50} = 40 nM; n = 4) and 6.3 ± 0.2 (IC_{50} = 540 nM, n = 3) in antagonizing β-arrestin recruitment and forskolin-induced cAMP, respectively (Fig. 1A).

In vitro pharmacological screening showed that the lead compound **81** has good solubility and can achieve concentrations ≥10 × IC_{50} in aqueous buffer between a pH range of 5.0–7.4

(Supplementry Table 3). Compound **81** also exhibited good PAMPA permeability, high plasma protein binding, excellent stability in mouse and human plasma and had a > 40-fold window for toxicity in human liver microsomes ($LC_{50} \geq 25$ μM). However, compound **81** was almost completely metabolized in human and mouse liver microsomes within 1h. Despite low *in vitro* microsomal stability, *in vivo* Rapid Assessment of Compound Exposure (RACE) assay with 10 mg/kg oral dose [DMSO: Tw80: H2O (1:1:8)] achieved good exposure and prompted us to carry out a full DMPK study in mice. Compound **81** had good bioavailability, clearance and exposure (clearance 28.4 mL/min/kg, Vdss 3.32 L/kg, t1/2 1.58 h after a 5 mg/kg intravenous dose, Cmax 798 ng/mL, t1/2 2.82 h, AUC 2047 ng·h/mL after a 10 mg/kg oral dose).

The murine CXCR6 receptor has 74% sequence homology with the human receptor. In addition, CXCL16 has only 46% species homology (https://blast.ncbi.nlm.nih.gov/Blast.cgi). ML339 probe had weak activity in antagonizing β-arrestin recruitment at the mouse CXCR6 receptor (IC_{50} = 18 μM)[8] and compound **81** was devoid of activity against the mouse receptor (IC_{50} > 40 μM, data not shown) indicating a limitation in validating *in vivo* activity in animal studies despite the compound's good bioavailability in mice. Therefore, we investigated human hepatoma cell lines to test functional activity of compound **81** *in vitro* and *in vivo* activity.

MicroRNA expression studies indicate CXCR6 expression and protein levels are about 2-fold greater in highly metastatic cells (MHCC97H, HCCLM3, and SK-HEP-1) compared with low metastatic Huh7, Hep3B cells and normal liver cell line L-02.[6] These studies also indicated that CXCR6 knockdown substantially inhibited invasive activity of hepatoma cells *in vitro* but had no impact on cell proliferation and cell-cycle distribution. Intriguingly, CXCL16, in its soluble form or transmembrane full-length form, could prominently promote control SK-HEP-1 and HCCLM3 cell invasion but not CXCR6-knockdown cells. Likewise, downregulation of CXCL16 markedly inhibited invasive activity of hepatoma cells *in vitro.* These results indicate that the contribution of CXCR6 on HCC cell invasion may be due to CXCR6-CXCL16 signaling and an autocrine loop of CXCL16 production. Thus, we examined SK-Hep-1 invasion using a live cell transwell assay. Compound **73** (Table 3) inhibited invasion while the inactive analog, compound **6** (Table 1), had no effect and compound **81** (Table 3) dose-dependently inhibited migration (IC_{50} = 2.1 μM) at 72 h without loss in cell viability (Supplementary Fig. 1A–C). Although there was not a significant difference in rate of migration between exogenous CXCL16 and serum control, this provided preliminary data for proof of concept testing in a SK-HEP-1 human xenograft mouse model.

We next evaluated the antitumor potential of compound **81** and the mechanism of CXCR6 inhibition in HCC xenograft model *in vivo* (Fig. 1B–D). SK-HEP-1 cells were injected subcutaneously into the flank region of female NOD/SCID mice on Day 1 for tumor development followed by oral administration of compound **81** initiated on Day 4 to Day 30. Treatment with the CXCR6 inhibitor at 30 and 60 mg/kg significantly inhibited SK-HEP-1 tumor growth compared to vehicle-treated animals ($P < 0.0005$ and 0.0002, respectively); cyclophosphamide (50 mg/kg) was used as a positive control (Fig. 1B). No deaths or behavior phenotypes were observed in all mice. Mice weight among four groups differed

indistinctly in SK-HEP-1 bearing mice (data not shown). We found that the weights of the excised SK-HEP-1 derived tumors treated with compound **81** at 30 and 60 mg/kg, respectively (59 ± 9 mg and 55 ± 24 mg) were significantly lighter than vehicle-treated tumors (151 ± 66 mg) ($P < 0.05$) and not significantly different in weight to cyclophosphamide-treated grafts (42 ± 24 mg) (Fig. 1C and D).

We report the discovery of a chemical series distinct from our previously reported probe molecule ML339 represented by compound **81** (Table 3). Compound **81** displays ≥ 10-fold improvement in potency in both the β-arrestin and cAMP assays (IC_{50} = 40 and 540 nM, respectively), inhibits migration of SK-HEP-1 hepatoma cells in a dose dependent manner and has promising oral DMPK data. Compound **81** is non-toxic to mice (30 and 60 mg/kg) and arrests tumor growth in SK-HEP-1 mouse xenografts to background levels similar to cyclophosphamide in a 30-day study and represents a promising pharmacological agent that may be used in more invasive mouse xenograft models to probe the CXCR6/CXCL16 axis in HCC.

Supplementary Material

Refer to Web version on PubMed Central for supplementary material.

Acknowledgements

We thank the cheminformatic and pharmacology cores at Sanford Burnham Prebys for providing compound management and ADME profiling support, respectively. We acknowledge Sang Bae at the University of Florida for providing scientific input and editing of the manuscript. The Molecular Structure Center at the Department of Chemistry, Indiana University, Bloomington graciously recorded and provided the X-ray structures. Finaly, we thank Altogen labs for helpful discussions in designing the xenograft study and WuXi AppTec (Shanghai) for pharmacokinetic data.

Funding

This work was funded by the Florida Translational Research Program (HTL0006), a contract administered by the Florida Department of Health. The funders provided support in the form of supplies and salaries for authors [S.P., P.M.H., R.J.K., E.S., P.R.M., E.H.S, D.D., C.J.M., D.T., L.H.S., S.M.], but did not have any additional role in the study design, data collection and analysis, decision to publish, or preparation of the manuscript. Earlier work focusing on the ML339 probe series was funded by the NIH Molecular Libraries Probe Production Centers network (MLPCN) grant # 1R03MH095589 (cycle 18)

References

1. Tabata S, Kadowaki N, Kitawaki T, et al. Distribution and kinetics of SR-PSOX/CXCL16 and CXCR6 expression on human dendritic cell subsets and CD4+ T cells. J Leukoc Biol. 2005;77:777–786. [PubMed: 15703197]
2. Heydtmann M, Lalor PF, Eksteen JA, Hübscher SG, Briskin M, Adams DH. CXC chemokine ligand 16 promotes integrin-mediated adhesion of liver-infiltrating lymphocytes to cholangiocytes and hepatocytes within the inflamed human liver. J Immunol. 2005;174:1055–1062. [PubMed: 15634930]
3. Geissmann F, Cameron TO, Sidobre S, et al. Intravascular immune surveillance by CXCR6+ NKT cells patrolling liver sinusoids. PLoS Biol. 2005;3:e113. [PubMed: 15799695]
4. Liang CM, Chen L, Hu H, et al. Chemokines and their receptors play important roles in the development of hepatocellular carcinoma. World J Hepatol. 2015;7:1390–1402. [PubMed: 26052384]

5. Ghouri YA, Mian I, Rowe JH. Review of hepatocellular carcinoma: epidemiology, etiology, and carcinogenesis. J Carcinog. 2017;16.

6. Gao Q, Zhao YJ, Wang XY, et al. CXCR6 upregulation contributes to a proinflammatory tumor microenvironment that drives metastasis and poor patient outcomes in hepatocellular carcinoma. Cancer Res. 2012;72:3546–3556. [PubMed: 22710437]

7. Sun JJ, Chen GY, Xie ZT. MicroRNA-361-5p Inhibits Cancer Cell Growth by Targeting CXCR6 in Hepatocellular Carcinoma. Cell Physiol Biochem. 2016;38:777–785. [PubMed: 26872014]

8. Hershberger PM, Peddibhotla S, Sugarman E, et al. Probing the CXCR6/CXCL16 axis: targeting prevention of prostate cancer metastasis. In: Health NIo, ed. Bethesda, MD: National Center for Biotechnology Information (US); 2010-. 2012:25.

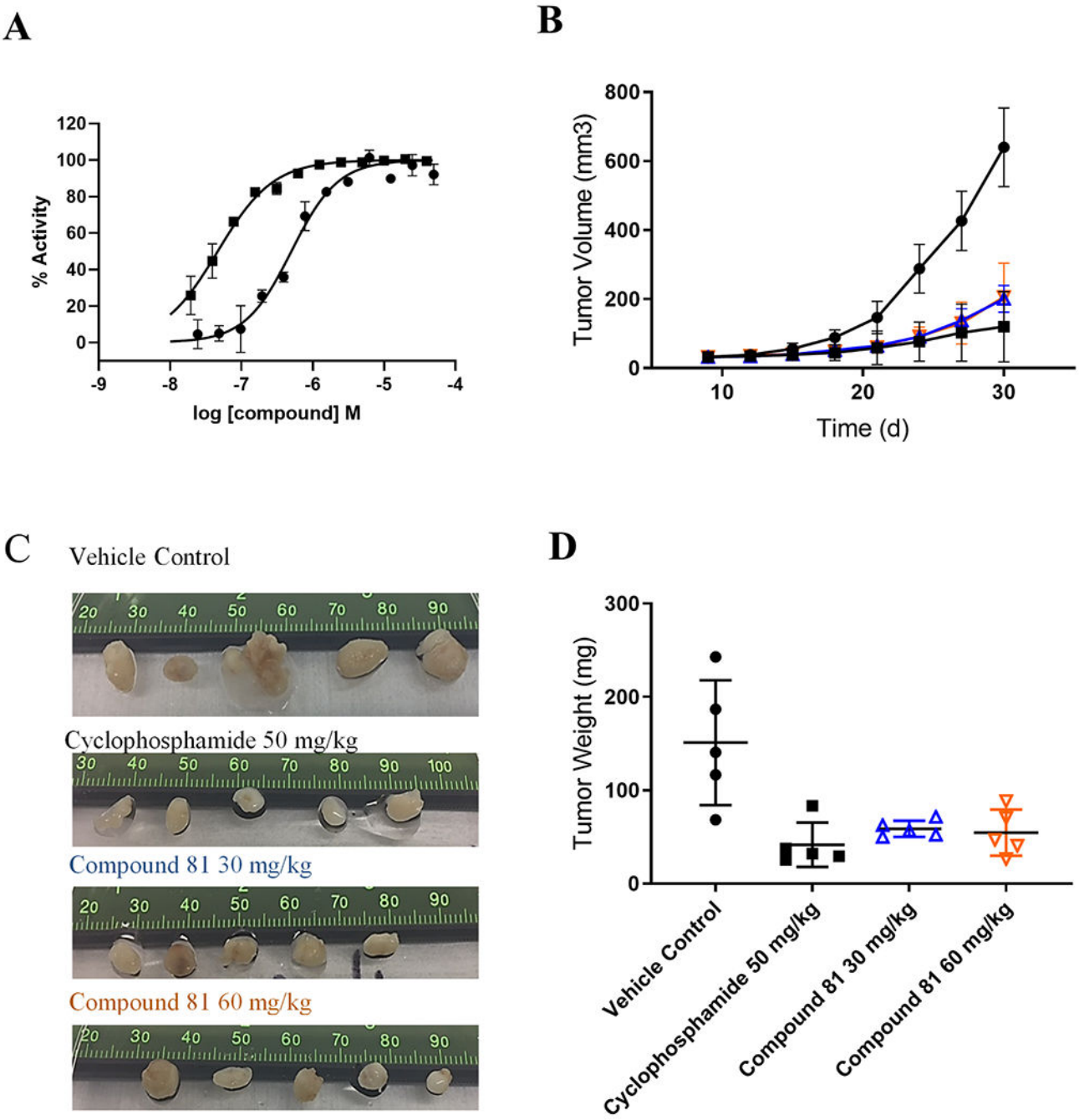

Fig. 1.

In vitro and *in vivo* activity of compound 81. (A) Inhibition of B-arrestin recruitment (squares) and forskolin-induced inhibition of CAMP production (circles) was determined using DiscoveRx cells expressing Prolink-tagged hCXCR6 treated with an EC_{80} concentration of CXCL16 and increasing concentrations of compound 81 (Table 3). (B) SK-HEP-1 induced tumor growth in mice over 30 days (closed circles) was inhibited by 30 mg/kg (blue triangles) and 60 mg/kg dose (red triangles) of compound 81. Cyclophosphamide at 50 mg/kg dose (closed squares) was used as a positive control. (C,D)

Tumors were removed from each animal to determine size and weight. Statistical significance of weight of 30 mg/kg and 60 mg/kg treatment groups compared to vehicle-treated was determined by student *t*-test ($P < 0.05$). (For interpretation of the references to colour in this figure legend, the reader is referred to the web version of this article.)

Table 1

SAR of Analogs of alternative scaffolds.

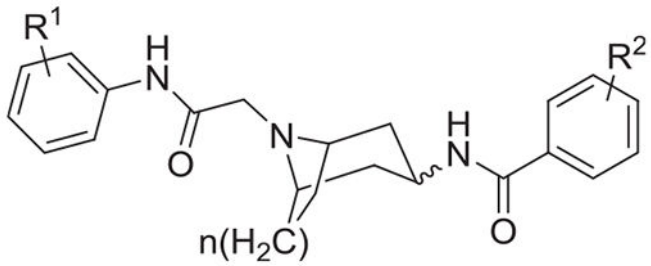

Entry	n	R_1	R_2	CXCR6: β-arrestin		CXCR6: cAMP	
				IC_{50} (μM)	% response	IC_{50} (μM)	% response
1Screen hit	3*	H	3,4,5-tri-OMe	5.8	65	30.6	86
2	3 endo	H	3,4,5-tri-OMe	> 40	NA	40.9	70
3	2*	H	3,4,5-tri-OMe	26	63	> 40	NA
4	2	H	3,4,5-tri-OMe	> 40	NA	> 40	NA
5	0	H	3,4,5-tri-OMe	> 40	NA	> 40	NA
6	3	H	H	> 40	NA	> 80	NA
7	3	4-F	3,4,5-tri-OMe	5.8	100	30.7	90
8	3	4-Cl	3,4,5-tri-OMe	1.5	101	14.2	93
9	3	4-Me	3,4,5-tri-OMe	9.5	100	> 40	NA
10	3	4-OMe	3,4,5-tri-OMe	19	76	> 40	NA
11	3	4-Cl	3,4-di- OMe	> 40	NA	> 40	NA
12	3	4-Cl	3,5-di-OMe	> 40	NA	> 40	NA
13	3	4-Cl	3-OMe	> 40	NA	14.5	87
14	3	4-Cl	4-OMe	> 40	NA	5.9	94
15	3	4-Cl	3,4-(OCH2O)	> 40	NA	5.3	84
16	3	2-F	3,4,5-tri-OMe	0.62	103	6.5	99
17 ML339	3	2-Cl	3,4,5-tri-OMe	0.14	100	1.4	102
18	3	2-Me	3,4,5-tri-OMe	0.79	104	9.3	101

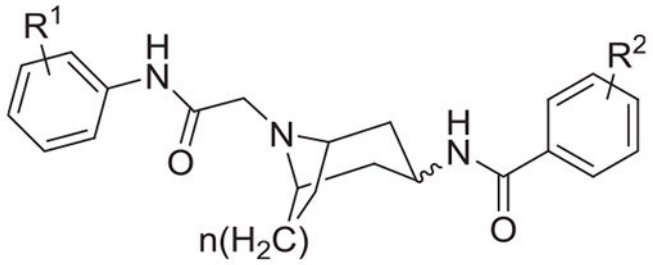

Entry	n	R_1	R_2	CXCR6: β-arrestin		CXCR6: cAMP	
				IC_{50} (μM)	% response	IC_{50} (μM)	% response
19	3	2-OMe	3,4,5-tri-OMe	2.1	102	14.7	100
20	3	2-Br	3,4,5-tri-OMe	0.16	105	0.9	104
21	3	2-CF_3	3,4,5-tri-OMe	0.64	101	7.9	105
22	3	2-CN	3,4,5-tri-OMe	0.93	91	7.0	105
23	3	2-CO2Et	3,4,5-tri-OMe	1.6	79	6.9	96
24	3	3-F	3,4,5-tri-OMe	0.84	104	8.5	103
25	3	3-Cl	3,4,5-tri-OMe	0.41	105	4.3	97
26	3	3-Br	3,4,5-tri-OMe	0.35	104	3.8	92
27	3	3-Me	3,4,5-tri-OMe	1.8	102	17.9	92
28	3	3-OMe	3,4,5-tri-OMe	5.8	96	51.0	93
29	3	2,3-dichloro	3,4,5-tri-OMe	0.16 0.12	102 96	0.41 25.6	78 39
30	3	2,4-dichloro	3,4,5-tri-OMe	0.16	105	0.9	105
31	3	2,5-dichloro	3,4,5-tri-OMe	0.13	99	0.7	101
32	3	2,6-dichloro	3,4,5-tri-OMe	38.2	57	> 40	NA
33	3	3,4-dichloro	3,4,5-tri-OMe	0.35	103	1.8	101
34	3	3,5-dichloro	3,4,5-tri-OMe	0.31	104	1.3	96
35	3	2,5-di Me	3,4,5-tri-OMe	0.61	105	16.5	108
36	3	2,6-di-Me	3,4,5-tri-OMe	> 40	NA	> 40	NA

*denotes exo configuration. All other entries are in the exo configuration.

Table 2

SAR of analogs of *exo-tert*-butyl-3-amino-9-azabicyclo[3.3.1]nonane-9-carboxylate.

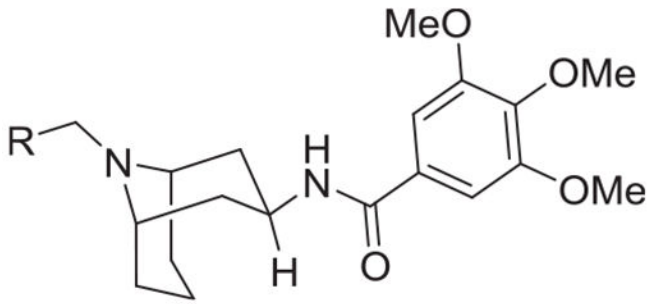

Entry	R	CXCR6: β-arrestin		CXCR6: cAMP	
		IC_{50} (μM)	% response	IC_{50} (μM)	% response
56	2-methoxyphenyl	> 50	NA	> 50	NA
57	3-methoxyphenyl	> 50	NA	> 50	NA
58	4-methoxyphenyl	> 50	NA	> 50	NA
59	2-chlorophenyl	6.8	99	11.5	101
60	3-chlorophenyl	9.5	97	14.8	100
61	4-chlorophenyl	23.7	90	38.6	58
62	2-napthyl	3.4	94	47.3	30
63	2-quinolinyl	6.7	88	40.3	88
64	2-indolyl	23.7	64	> 50	NA
65	3-indolyl	> 50	NA	> 50	NA
66	2-imidazo [1,2-*a*] pyridine	> 50	NA	> 50	NA
67	2-benzothiophenyl	0.9	93	25.0	49
68	2-benzothiazolyl	0.3	101	7.9	85
69	2-benzoxazolyl	6.9	83	> 50	26
70	2-benzimidazolyl	10.5	84	> 40	NA
71	2-benzothiazolylmethyl	> 50	NA	> 50	NA
72	benzothiazole-2-carbonyl	12.7	75	> 50	NA

Table 3

SAR of benzothiazole analogs.

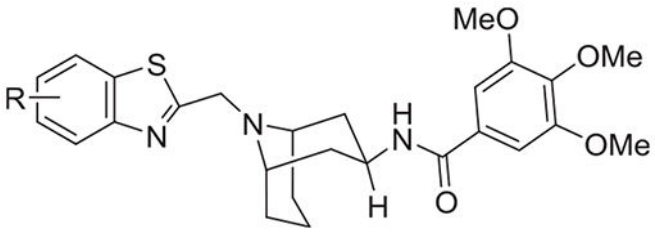

Entry	R	CXCR6: β-arrestin		CXCR6: cAMP	
		IC_{50} (μM)	% response	IC_{50} (μM)	% response
73	4-Cl	0.13	103	0.9	95
74	5-Cl	0.17	100	3.2	90
75	6-Cl	0.27	103	14.0	83
76	7-Cl	0.26	102	8.9	93
77	4-F	0.11	103	1.9	105
78	4-Me	0.25	100	4.8	86
79	4-OMe	3.1	86	> 50	NA
80	4-Br	0.08	102	1.0	91
81	4-CF_3	0.04	103	0.5	98